Gated-charge force microscopy for imaging a surface-acoustic-wave-induced charge in a depleted one-dimensional channel

R. Crook,* R. J. Schneble, M. Kataoka, H. E. Beere, D. A. Ritchie, D. Anderson, G. A. C. Jones, C. G. Smith, C. J. B. Ford, and C. H. W. Barnes

Cavendish Laboratory, 19 J J Thomson Avenue, Cambridge CB3 0HE, United Kingdom

(Received 21 August 2008; published 30 September 2008; corrected 14 October 2008)

Gated-charge force microscopy (GCFM) generates images of subsurface induced charge with single-electron charge resolution and zero sensitivity to background charge, for the noninvasive study of confined quantum electronic systems. By gating the radio-frequency signal applied to transducers, which generate surface-acoustic waves (SAWs), we use GCFM to generate images of a GaAs depleted one-dimensional channel and provide insight to SAW-induced transport. Unexpected SAW-induced subsurface charge was imaged at points of high potential gradient. This suggests that electrons depopulating a SAW minimum due to a high potential gradient rapidly lose energy and interact with following SAW minima.

DOI: 10.1103/PhysRevB.78.125330 PACS number(s): 73.23.−b, 85.50.−n, 07.79.−v

I. INTRODUCTION

Scanning-probe microscopy has provided unique and valuable insights into many subsurface low-temperature quantum phenomena.[1–8] For example, dynamic-force techniques where the mechanical resonant properties of a cantilever and tip are used to detect the small electrostatic force between the tip and sample have been used to measure the electric potential of subsurface two-dimensional electron systems (2DESs) in the quantum Hall regime.[1,2] Charge induced on a scanning probe tip has also been detected electrically.[3,4] A limitation of such dynamic-force techniques, when imaging highly confined quantum systems such as dots and wires, is the presence of a background signal associated with the electrodes or etched regions that are used to define the quantum system being studied. The spatial variation in the background signal is often orders of magnitude greater than the desired device signal, leading to poor measurement sensitivity due to the forced selection of a nonoptimal instrument range and difficulties during image processing when separating the background and device signals. Scanning-gate microscopy (SGM), where the conductance of a subsurface electron system is measured in response to the potential perturbation from a scanning biased tip, is largely immune to such background signals and has been used to investigate electronic transport through confined quantum systems including channels,[5] billiards,[6] rings,[7] dots,[8] and nanotube dots.[9] However, SGM measures the quantum system response to the tip perturbation and consequentially generates images from which it is difficult to infer unperturbed subsurface charge density.

In this paper we demonstrate gated-charge force microscopy (GCFM). This noninvasive dynamic-force technique generates images of subsurface charge in confined systems with single-electron charge resolution and zero sensitivity to background charge. Only a dc bias is applied to the tip, and the cantilever is not driven mechanically. A mechanism is used to periodically remove and then replace the charge in the confined system. The electrostatic force between charge on the tip and the periodic system charge drives the cantilever near resonance, and the cantilever oscillation amplitude and phase are recorded using lock-in techniques. All background charge is static and therefore not detected. Gating of charge is achieved here by gating the radio-frequency (RF) signal applied to surface-acoustic-wave (SAW) transducers. Single electrons or a small discrete number of electrons are trapped and transported in the potential troughs associated with the SAWs propagating past depleted channels.[10,11] Gating the RF signal therefore gates the flow of charge to and through the channel. The technique is also insensitive to the (unpopulated) SAW potential itself because the time average of the SAW potential is zero. The images reveal the presence of charge within the channel coincident with regions of high potential gradient, which suggests that electrons rapidly lose energy and interact with the potential troughs of following SAWs.

II. CALCULATION AND EXPERIMENTAL METHOD

Our system is modeled as a parallel-plate conductive tip positioned above a time-periodic point charge $q(t)=q_0+q_1\cos(\omega t)+\ldots$ buried in a dielectric substrate. Using the method of images and geometric approximations, similar to Krauss and Brus,[12] the oscillatory force at frequency ω between the tip and the point charge is

$$F_\omega = \frac{q_1\alpha}{4\pi\varepsilon_0(s+h)^2}\left(-\frac{5C(V_{\mathrm{tip}}+\phi)}{4}+\frac{q_0\alpha}{2}\right). \qquad (1)$$

C is the capacitance between the tip and any underlying 2DES, s is the separation between the tip and surface, h is the depth of the point charge, V_{tip} is a dc bias applied between the tip and 2DES, and ϕ is the contact potential difference between tip and sample materials. The dielectric substrate, in which $\varepsilon=\varepsilon_0\varepsilon_1$, is incorporated with $\alpha=2\varepsilon_1/(1+\varepsilon_1)$. An image charge of size $-\alpha q$ is assumed to exist within the tip a distance $s+h$ from the tip's surface. The terms within the brackets in Eq. (1), respectively, account for capacitive and Coulombic origins. The capacitive term combines the forces between charge applied by $V_{\mathrm{tip}}+\phi$ on either the tip or 2DES and the point charge or its image, respectively. The Coulombic term represents the force between the point charge and its image.

Figure 1 illustrates the experiment. A 2DES was formed at a GaAs/AlGaAs heterojunction 90 nm beneath the surface

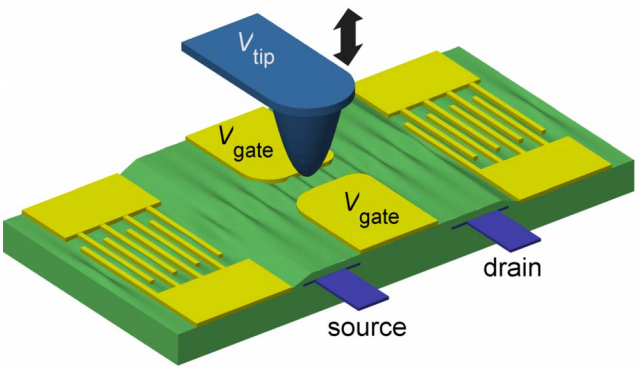

FIG. 1. (Color online) Illustration of experimental setup. Surface acoustic waves were generated by applying a RF signal to the interdigitated-finger transducer at the left-hand end of the device. The SAW channel was defined from the 2DES by applying a negative bias to the central gate electrodes. Source and drain ohmic contacts connect to the 2DES.

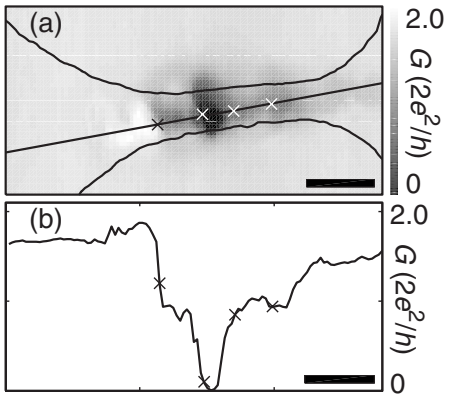

FIG. 2. (a) SGM (device conductance) image of the SAW channel made with $V_{tip}=-1.6$ V and $V_{gate}=-0.9$ V. The contour outlines the gate electrodes. Four crosses locate spots of charge seen in subsequent GCFM images. (b) Conductance profile along the length of the SAW channel, following the line shown in (a). Data were taken at 400 mK in the absence of SAWs. Scale bars are 1 μm.

with mobility 350 $m^2\,V^{-1}\,s^{-1}$ and electron density 3.7×10^{15} m^{-2} after 1 s illumination from a red LED. The SAW channel was defined from the 2DES by applying a negative bias to surface electrodes fabricated in a split-gate configuration. The channel was lithographically 2-μm long and 0.7-μm wide, with radii of curvature at the entrance and exit of 4 μm and 2 μm, respectively. For the piezoresistive cantilever used throughout these experiments, the resonant frequency is 71.623 kHz and the Q factor is 2×10^4 in vacuum at 400 mK. SAWs, with a wavelength of 1.0 μm, were generated by applying a 2.7532 GHz RF signal to an interdigitated-finger transducer, which was fabricated over a region etched below the 2DES located 2.5 mm to the left of the SAW channel. The RF signal amplitude was 17 dBm but the signal reaching the transducer was attenuated due to losses in the cables and poor impedance matching between the cable and the transducer. To reduce sample heating,[13,14] the gating-signal pulse width was limited to 2 μs at a frequency of 71.633 kHz. The SAW-induced current was measured through the drain ohmic contact by the direct connection to a dc 50 pA V^{-1} transresistance amplifier. A −0.3 mV dc bias was applied to the source ohmic contact to compensate for the amplifier input bias.

III. EXPERIMENTAL IMAGES

The SGM image (of device conductance) presented in Fig. 2(a) shows that the channel is not uniform. Figure 2(b) provides a conductance profile along the length of the SAW channel, which is known to be representative of the device potential profile.[15] Although this profile was necessarily made with the channel conductive, a similar, but less well screened device potential profile will persist when the channel is depleted. The contour shown on all the images is reproduced from an electrostatic force microscopy (EFM) image[2,12,16] generated by applying an ac bias to the 2DES via the source and the drain ohmic contacts. The contour with a channel width equal to the lithographic channel width was chosen. When the tip is positioned over surface gates, which are held at a constant bias, the capacitance from the tip to the 2DES is reduced due to screening by the gates. The EFM image reveals the spatial dependence of $\partial C/\partial z$ and can therefore be used to precisely locate the surface electrodes.

Figure 3 presents a series of GCFM images with V_{gate} decreasing from −1.00 to −1.30 V. The source and drain ohmic contacts were connected to 0 V, and $V_{tip}=-0.6$ V was chosen to minimize the tip potential perturbation in the 2DES plane. The tip scanned 20 nm above the sample surface. Each image reveals a different pattern of spots, identifying the locations of SAW-induced charge. Four locations where charge is repeatedly observed are marked by four crosses on the images. The same locations are identified on the SGM image and profile of Fig. 2. Additional GCFM images were generated with the RF signal frequency shifted so that SAW standing waves, if they had existed, would move by 0.5 and 0.25 SAW wavelengths. Images were also generated with both shorter and longer SAW pulses. Features in all the additional images were qualitatively identical, ruling out interference effects as the origin of features seen in the images. The spacing between the spots of charge is unequal and averages at 0.8 times the SAW wavelength. Figure 4 plots device SAW current and device conductance as functions of V_{gate} and also plots the range of SAW-induced charge from each of the images in Fig. 3.

IV. IMAGE CALIBRATION AND DISCUSSION

Calibration of the GCFM images proceeds by modeling the worn-tip-2DES system as a parallel-plate capacitor. The radius of the tip is approximately 50 nm and the tip bias required to null features in the GCFM images provides $\phi=0.8$ V. The Fourier series of the pulse-modulated SAW provides $q_0=-0.143ne$ and $q_1=-0.276ne$, where $-ne$ is the SAW-induced charge when the SAW is present. With $n=1$, Eq. (1) gives $F_\omega=0.04$ pN, meaning the white features in the images in Fig. 3 correspond to a SAW-induced charge of approximately $-e$. Depletion of the 2DES will reduce C, so

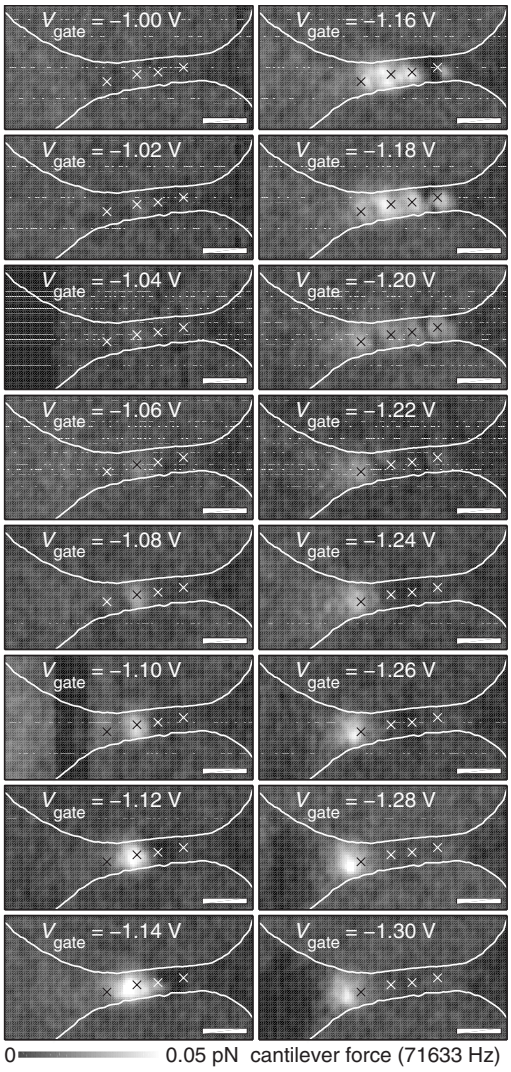

FIG. 3. Series of GCFM images for V_{gate} from −1.00 to −1.30 V with V_{tip}=−0.6 V. A small background level has been subtracted from each image independently. The range of electric potential is the same in all images. The contour outlines the gate electrodes and four crosses locate points where SAW-induced charge is prevalent. Data were taken at 400 mK. Scale bars are 1 μm.

the charge calibration is likely to be an underestimate in regions where the channel is highly depleted.

A critical observation is that the two leftmost charge spots (crosses) spatially align with regions of high potential gradient within the channel, as is evident from Fig. 2(b). This provides a valuable insight for SAW-induced transport. Consider two scenarios for the fate of electrons depopulated from SAW minima due to a high potential gradient.[16–18] In the *hot-electron* scenario, electrons rapidly leave the channel region and equilibrate their energy with the 2DES. In the *thermalization* scenario, electrons lose their energy sufficiently fast so they can interact with the adjacent SAW minima and associated electrons with the possibility of being captured in the following SAW minimum. A classical time-stepping simulation was performed to see which of these scenarios is compatible with the experimental GCFM images. The position of electrons were tracked under the combined electric field of a sinusoidal SAW potential, a smoothed-step device potential, and the Coulombic potential of all other electrons. The simulation used a SAW channel of sufficient length so that end effects, such as screening from the 2DES, could be ignored. A velocity damping term was included for the thermalization scenario only.

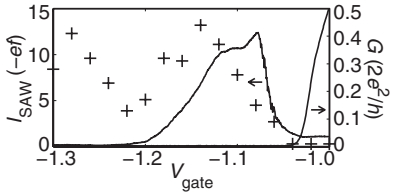

FIG. 4. Plot of SAW current and device conductance as a function of V_{gate} made with the tip retracted (V_{tip}=−0.6 V). The plus symbols plot the relative range (signal to noise) from the GCFM images of Fig. 3 (the signal-to-noise ratio is 0 at V_{gate}=−1.00 V and is maximum at 4.4 at V_{gate}=−1.14 V). Data were taken at 400 mK.

Using the thermalization scenario, it was possible to simulate regions of high charge density associated with both positive (uphill) and negative (downhill) potential gradients. At regions of positive potential gradient, each electron fell back into the following SAW minimum but the electron was nevertheless transported over the gradient to be available to generate further charge-density features. The increase in local charge density was several times the background level (smoothed over 200 nm). At regions of negative gradient, the electron position fluctuates within a single minimum, which leads to a spatial fluctuation in charge density of smaller magnitude than at a positive gradient. The simulation reproduced all features of the experimental GCFM images. Using the hot-electron scenario, it was not possible to simulate a suitably large charge density or a series of charge spots consistent with the experimental GCFM images. This suggests that electrons depopulating a SAW minimum due to a high potential gradient rapidly lose energy and interact with adjacent SAW minima.

Returning to Fig. 3, the evolution of the GCFM images with V_{gate} can now be interpreted under four regimes. From V_{gate}=−1.00 to −1.04 V, the channel is conductive and transport electrons screen the SAW potential. The SAW-induced current is zero and the images show only noise. From V_{gate}=−1.06 to −1.14 V, a short depleted region forms in the central part of the channel only. The conductance falls to zero and the SAW-induced current increases to a peak of $-13ef$, where f is the SAW frequency.[10,11] The images reveal significant SAW-induced charge associated with the high positive potential gradient of the depleted region. It is not clear why charge is not associated with the adjacent negative potential gradient. From $-V_{gate}$=−1.16 to −1.20 V, the depleted region lengthens and the SAW current falls to a small multiple of $-ef$. This is the regime where devices that utilize SAW-induced transport would normally operate. Up to four simultaneous spots of SAW-induced charge are seen and are associated with four regions of high potential gradient (positive and negative). Beyond V_{gate}=−1.22 V, the potential gradient near the channel entrance is sufficiently large to com-

pletely depopulate the SAW potential minima so the SAW current falls to zero. The images reveal a single region of charge tracking the channel entrance, which moves to the left as the depleted region lengthens. Under this regime it might be expected that a significant charge should build up at the channel entrance particularly as the width of the channel entrance increases. Charge is delivered by successive SAW minima and the fact that the SAW current is zero suggests charge is unable to leave. There is evidence of this effect in Fig. 4 for gate voltages more negative than −1.22 V where a general upward trend in GCFM peak signal is seen. However, the effect is likely to be limited by strong screening from the 2DES, which rapidly diminishes the SAW potential amplitude and therefore, the ability to maintain charge in a SAW minimum in the entrance and exit regions.

V. CONCLUSION

GCFM has been used to generate a series of images of a GaAs depleted one-dimensional channel. The technique has single-electron charge resolution and is insensitive to background charge making it appropriate for the study of highly confined quantum systems. In this case, charge was gated by modulating the RF signal applied to SAW transducers to therefore modulate the presence of SAWs propagating through the device. Each image revealed a set of spots caused by SAW-induced charge, which are shown to coincide with regions of high potential gradient in the device. Depopulation of the SAW minima is considered in two scenarios. In the hot-electron scenario electrons rapidly leave the channel and equilibrate their energy with the 2DES. In the thermalization scenario electrons lose their energy sufficiently fast so they can interact with the following SAW minima. Only under the thermalization scenario are features of the experimental images reproduced using a classical time-stepping simulation.

Finally, consider how GCFM can be used to image charge in quantum devices that do not utilize SAW-induced transport. System charge must modulate at the gating-signal frequency, direct coupling between the gating signal and the tip must be kept to a minimum, and screening from 2DES electrons must be ineffective. This could be achieved by applying an electrical gating signal to a remote surface electrode to control a flow of hot electrons (nonequilibrium electrons) that subsequently populate a depleted quantum system such as a quantum dot or channel.[19] An optically gated implementation can also be envisaged where optically excited electrons momentarily populate the quantum system. While single-electron charge resolution is demonstrated here, there is scope to improve charge resolution further. For example, the duty cycle of the gating signal was necessarily limited to 14%. Charge sensitivity can be improved by a factor of 3 by using the optimum duty cycle of 65%. These experiments also demonstrate that a nonuniform distribution of charge can exist in a SAW channel, which should be considered during the design of advanced devices based on SAW-induced transport.[20]

ACKNOWLEDGMENTS

This research is part of the QIP IRC (www.qipirc.org) supported by the UK EPSRC (Grant No. GR/S82176/01).

*Current address: ERRI, Faculty of Engineering, University of Leeds, Leeds LS2 9JT, United Kingdom.

[1] K. L. McCormick, M. T. Woodside, M. Huang, M. Wu, and P. L. McEuen, Phys. Rev. B **59**, 4654 (1999).
[2] P. Weitz, E. Ahlswede, J. Weis, K. v. Klitzing, and K. Eberl, Appl. Surf. Sci. **157**, 349 (2000).
[3] S. H. Tessmer, P. I. Glicofridis, R. C. Ashoori, L. S. Levitov, and M. R. Melloch, Nature (London) **392**, 51 (1998).
[4] G. A. Steele, R. C. Ashoori, L. N. Pfeiffer, and K. W. West, Phys. Rev. Lett. **95**, 136804 (2005).
[5] M. A. Topinka, B. J. LeRoy, S. E. J. Shaw, E. J. Heller, R. M. Westervelt, K. D. Maranowski, and A. C. Gossard, Science **289**, 2323 (2000).
[6] R. Crook, C. G. Smith, A. C. Graham, I. Farrer, H. E. Beere, and D. A. Ritchie, Phys. Rev. Lett. **91**, 246803 (2003).
[7] B. Hackens, F. Martins, T. Ouisse, H. Sellier, S. Bollaert, X. Wallart, A. Cappy, J. Chevrier, V. Bayot, and S. Huant, Nat. Phys. **2**, 826 (2006).
[8] A. Pioda, S. Kičin, T. Ihn, M. Sigrist, A. Fuhrer, K. Ensslin, A. Weichselbaum, S. E. Ulloa, M. Reinwald, and W. Wegscheider, Phys. Rev. Lett. **93**, 216801 (2004).
[9] M. T. Woodside and P. L. McEuen, Science **296**, 1098 (2002).
[10] J. M. Shilton, V. I. Talyanskii, M. Pepper, D. A. Ritchie, J. E. F. Frost, C. J. B. Ford, C. G. Smith, and G. A. C. Jones, J. Phys.: Condens. Matter **8**, L531 (1996).
[11] T. J. M. Janssen and A. Hartland, Physica B **284-288**, 1790 (2000).
[12] T. D. Krauss and L. E. Brus, Phys. Rev. Lett. **83**, 4840 (1999).
[13] R. J. Schneble, M. Kataoka, C. J. B. Ford, C. H. W. Barnes, D. Anderson, G. A. C. Jones, I. Farrer, D. A. Ritchie, and M. Pepper, Appl. Phys. Lett. **89**, 122104 (2006).
[14] M. Kataoka, C. J. B. Ford, C. H. W. Barnes, D. Anderson, G. A. C. Jones, H. E. Beere, D. A. Ritchie, and M. Pepper, J. Appl. Phys. **100**, 063710 (2006).
[15] R. Crook, C. G. Smith, M. Y. Simmons, and D. A. Ritchie, Physica E (Amsterdam) **12**, 695 (2002).
[16] R. Crook, R. J. Schneble, M. Kataoka, H. E. Beere, D. A. Ritchie, D. Anderson, G. A. C. Jones, C. G. Smith, C. J. B. Ford, and C. H. W. Barnes (unpublished).
[17] M. Kataoka, C. H. W. Barnes, H. E. Beere, D. A. Ritchie, and M. Pepper, Phys. Rev. B **74**, 085302 (2006).
[18] A. M. Robinson and C. H. W. Barnes, Phys. Rev. B **63**, 165418 (2001).
[19] K. Furuya, Y. Ninomiya, N. Machida, and Y. Miyamoto, Phys. Rev. Lett. **91**, 216803 (2003).
[20] C. H. W. Barnes, J. M. Shilton, and A. M. Robinson, Phys. Rev. B **62**, 8410 (2000).